IEEE Access
Multidisciplinary | Rapid Review | Open Access Journal

Received August 4, 2019, accepted September 3, 2019, date of publication September 13, 2019, date of current version October 1, 2019.

Digital Object Identifier 10.1109/ACCESS.2019.2941203

A Channel Calibration Algorithm Based on Isolated Scatterers for Multi-Channel HRWS-SAR

DI WU[1,2], YUDONG ZHANG[3], (Member, IEEE), DAIYIN ZHU[1], (Member, IEEE), SHUIHUA WANG[4], (Member, IEEE), AND MINGWEI SHEN[5]

[1]Key Laboratory of Radar Imaging and Microwave Photonics, Ministry of Education, Nanjing University of Aeronautics and Astronautics, Nanjing 210016, China
[2]Key Laboratory of Dynamic Cognitive System of Electromagnetic Spectrum Space, Ministry of Industry and Information Technology, Nanjing University of Aeronautics and Astronautics, Nanjing 211106, China
[3]Department of Informatics, University of Leicester, Leicester LE1 7RH, U.K.
[4]Department of Mathematics, University of Leicester, Leicester LE1 7RH, U.K.
[5]College of Computer and Information, Hohai University, Nanjing 211100, China

Corresponding author: Di Wu (wudi82@nuaa.edu.cn)

This work was supported in part by the Aeronautical Science Foundation of China under Grant 20162052019, in part by the China Scholarship Council under Grant 201806835006, in part by the National Natural Science Foundation of China under Grant 61771182, and in part by the Qing Lan Project of Jiangsu, China.

ABSTRACT Multi-channel receiving technique has been proved to be a promising approach for synthetic aperture radar (SAR) to achieve simultaneous high-resolution and wide-swath (HRWS) imaging. With the support of digital beamforming (DBF) technique, ambiguity-free signal can be reconstructed from the Doppler aliased data received by along-track channels with high fidelity. However, in practice, a key factor that affects the precision of spectrum reconstruction and deteriorates the quality of final image is the inevitable mismatch between receiving channels. Thus, channel calibration is recognized as a crucial step prior to DBF. In this paper, we propose a novel channel calibration algorithm for multi-channel HRWS-SAR system. Instead of using signal subspace projection or other matrix decomposition methods adopted in most of the existing HRWS-SAR channel calibration algorithms, it tries to find ambiguity-free ''sample signal'' to be used in the estimation of channel error directly from the original Doppler ambiguous data. We demonstrate that, by applying sub-aperture operation to the original data, unambiguous multi-channel signal corresponding to isolated ground scatterers can be extracted, and thereby can be utilized to accurately estimate and calibrate the azimuth-variant channel mismatch. Experimental results from a four-channel and a three-channel airborne SAR systems are employed to validate the effectiveness and robustness of the proposed algorithm in practical processing.

INDEX TERMS Synthetic aperture radar (SAR), high-resolution wide-swath (HRWS), multi-channel, channel calibration, sub-aperture processing.

I. INTRODUCTION

Equipped with a multi-channel receiving antenna, synthetic aperture radar (SAR) mounted on high-speed moving platform (such as satellite and near space vehicle) gains the ability to overcome the constraint of minimum antenna area, and hence can acquire simultaneous high-resolution and wide-swath (HRWS) radar images [1]–[8]. An intuitive explanation for this advantage is that the spatial sampling achieved by multi-channel receiving technique can provide additional samples between neighboring pulses in slow-time domain, which is equivalent to increasing the pulse repetition frequency (PRF) of the system. This procedure is also referred to as the reconstruction of ambiguity-free Doppler spectrum in literature, recognized as the most crucial step in multi-channel HRWS-SAR signal processing.

Considering the too strict displaced phase center antenna (DPCA) condition [1] and many other uncertain factors in practical applications, Doppler spectrum reconstruction in multi-channel SAR is usually operated in range-Doppler (RD) domain via cross-channel digital beamforming (DBF) approaches [1]–[3]. The DBF techniques combine the signal from different receiving channels and then filter them by spatial filter banks, making the mitigation of

The associate editor coordinating the review of this manuscript and approving it for publication was Guolong Cui.

azimuth ambiguities more flexible [4]. To gain even better robustness in different environments, DBF with adaptive processing, referred to as adaptive digital beamforming (ADBF) or space-time adaptive processing (STAP), are also proposed in [5]–[8] to reconstruct the unambiguous Doppler spectrum. The performance of DBF for HRWS-SAR has already been verified by the ground-based multi-channel SAR demonstrator [9], the airborne experimental system, i.e., F-SAR in DLR [10], and also the spaceborne system TerraSAR-X [4], [11], and RADARSAT-2 [7], [12], [13].

However, a key factor that limits the performance of DBF for multi-channel HRWS-SAR is the inevitable imbalance between different receiving channels, which is also referred to as channel mismatch or channel error. In practice, channel mismatch usually appears to be range and azimuth-variant, and can be caused by a variety of reasons, such as the difference in antenna gains, inaccurate locations of antenna centers, unsynchronized sampling time between channels, and so on. The quality of final SAR image will suffer a significant deterioration if all the receiving channels are not well calibrated prior to DBF processing.

In fact, the issue of channel calibration has long been addressed in research field of multi-channel SAR ground moving target indication (GMTI) with a number of mature techniques proposed, such as the signal subspace method proposed in [14], the two-dimensional (2D) frequency domain iterative method provided in [15] and the principal eigenvector method mentioned in [16] and [17, Chapter 13]. Most of these methods are data-based that can automatically estimate channel error from received data and are proved to be effective and robust when processing real data.

However, when it comes to HRWS-SAR system, all these methods suffer from their inability to accurately calibrate channel mismatch. As we know, in most of the calibration algorithms for SAR-GMTI system (where Doppler ambiguity is assumed to be absent), a key underlying assumption is the single-valued coupling relationship between azimuth and Doppler [18]. Based on that, antenna responses corresponding to each receiving channel, also referred to as array manifold [17], are estimated from the received data in Doppler (or image) domain and used for the following calibration. While, due to the Doppler ambiguity, the single-valued relationship is no longer established in HRWS-SAR system, leading to the invalidation of these methods.

To remedy this, new channel calibration algorithms for multi-channel HRWS-SAR in case of Doppler ambiguity were proposed in the past years [6], [19]–[28]. In [6], a data-based automatic channel calibration algorithm was proposed for distributed small satellite SAR system. This algorithm decomposes channel mismatch into different components as gain, phase, and antenna position errors. By considering the orthogonality between signal and noise subspace, an iterative subspace projection approach is utilized to estimate each kind of errors. Based on this work, an improved subspace projection algorithm was proposed in [19], where range-variant and azimuth-variant errors are calibrated separately in two steps and the iterative processes is totally avoided. Thus, it is more robust to range-variant channel mismatch and computational efficient as compared to the algorithm in [6]. In [20], based on the assumption that the steering vectors in one Doppler bin are conjugate with those in its contrary Doppler bin, a new calibration algorithm was presented to estimate the phase errors between channels, which also avoid iterative processes in subspace projection processing, and hence reduces the computational burden. In [21] and [22], algorithms with improved performance were proposed, where the entire calibration procedure is divided into two steps, i.e., the coarse calibration and the fine calibration. The range sampling time error and gain-phase error are calibrated in the first step, while the residue error is divided into several components, which are accurately calibrated using local maximum-likelihood weighted minimum entropy methods. Moreover, algorithms based on azimuth cross-correlation [23]–[25] and many others [26]–[29] were also provided to effectively deal with different kinds of channel mismatches.

All the above mentioned methods have been theoretically proved to be promising for HRWS-SAR system and many of them are validated by measured data. However, there still exist some performance limitations. As we know, most of these algorithms are based on signal subspace projection or other matrix decomposition methods. When the total number of ambiguities is close to the freedom of system (the number of receiving channels), the signal subspace occupied by signal from different Doppler centers will appear to be crowded, which may affect the precision of the subspace projection. Moreover, in some of these algorithms, channel mismatch are divided into different components modeled via a series of parameters, which means that the parametric models are employed in the estimation of channel error. Hence, similar to most of other parametric estimation approaches, they may not be robust to fast-varying or high-order error that deviates from the parametric model.

This paper tackles the channel calibration problem for multi-channel HRWS-SAR in a totally different way as compared to the methods mentioned above. Instead of focusing on the analysis of signal and noise subspaces or other matrix decomposition approaches, we propose to extract some ambiguity-free multi-channel signal directly from the original Doppler aliased data, which are then used as "samples" to estimate the real array manifold and the channel error. Since all the receiving channels should be involved in the estimation of channel mismatch, any DBF or other array signal processing method that may combine the signal from different channels cannot be adopted in this procedure. It seems to be impossible, at first sight, to reconstruct the unambiguous signal without the support of array processing. However, as it will be demonstrated in this paper, at least, the multi-channel signal concerning isolated ground scatterers (point-like targets) can be reconstructed without Doppler ambiguity via sub-aperture processing method. Based on that, we propose here a new channel calibration algorithm for

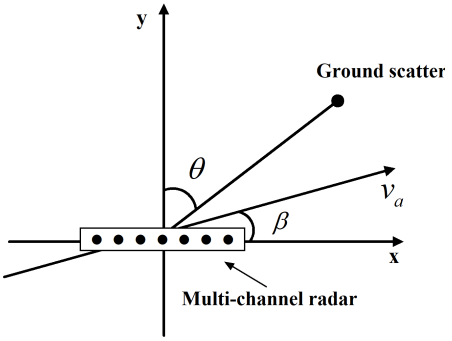

FIGURE 1. Simplified geometry for multi-channel HRWS-SAR.

multi-channel HRWS-SAR and validate it via experimental results.

The rest of this paper is organized as follows. In section II, the signal model of multi-channel HRWS-SAR is established when Doppler ambiguity is absent and present in the receiving data. In section III, classical ADBF methods for multi-channel HRWS-SAR are reviewed, and the influence of channel mismatch is also discussed. In section IV, the new channel calibration algorithm is proposed. The signal processing flow, especially the operation to extract ambiguity-free signal corresponding to isolated scatterers is described in detail. In section V, experimental results obtained from two multi-channel airborne SAR systems are employed to validate the effectiveness of the proposed algorithm. Finally, section VI provides a conclusion.

II. SIGNAL MODEL OF MULTI-CHANNEL HRWS-SAR

A simplified two-dimensional (2D) geometry for multi-channel HRWS-SAR is shown in Fig.1. A multi-channel SAR system with N receiving channels is mounted on a moving platform flying at a constant velocity denoted by v_a. The x-axis where the receiving channels lie on makes a crab angle denoted by β with the platform velocity vector and the y-axis points the normal direction of the multi-channel antenna. For the ground scatterer localized at azimuth direction denoted by θ, the instantaneous Doppler frequency induced by platform motion is obtained from

$$f_d = \frac{2v_a \cos\left(\frac{\pi}{2} - \theta - \beta\right)}{\lambda} = \frac{2v_a \sin\left(\theta + \beta\right)}{\lambda} \tag{1}$$

where λ is the radar wavelength.

Equation (1) that reveals the Doppler-azimuth coupling effect for moving radar system [18], is recognized as an important fundamental principle for airborne/spaceborne radars working at air-to-ground model. When the crab angle is not too large (in side-looking or squint-looking models) and the antenna beam is not too wide in azimuth, the Doppler-azimuth relationship appears to be single-valued, making it possible for us to observe radar measurements depending on azimuth or to estimate azimuth-variant parameters in Doppler domain.

Consider now the receiving channels are uniformly separated, with d denoting the distance between each other, and assume that every channel receives signal independently. The array response to the scatterer localized at azimuth θ, i.e., the spatial steering vector, can then be expressed as

$$\mathbf{s}\left(\theta\right) = \left[s_1\left(\theta\right), s_2\left(\theta\right), \cdots, s_N\left(\theta\right)\right]^T = \mathbf{g}\left(\theta\right) \odot \mathbf{v}\left(\theta\right) \tag{2}$$

where $\mathbf{g}\left(\theta\right) = \left[g_1\left(\theta\right), g_2\left(\theta\right), \cdots, g_N\left(\theta\right)\right]^T$ is the vector represents the amplitude and phase mismatches between channels, with $g_i\left(\theta\right), i = 1, 2, \cdots N$, denoting the mismatch term on the ith channel, the superscript T denotes the transpose operation, $\odot$ stands for the Hadamard product, and $\mathbf{v}\left(\theta\right)$ is the ideal steering vector (for which the channel mismatch is assumed to be absent) with respect to azimuth θ denoted by

$$\mathbf{v}\left(\theta\right) = \left[1, e^{\frac{j2\pi d}{\lambda}\sin(\theta)}, \cdots, e^{\frac{j2\pi d(N-1)}{\lambda}\sin(\theta)}\right]^T. \tag{3}$$

When there is no mismatch between receiving channels or all the channels are perfectly calibrated, the vector $\mathbf{g}\left(\theta\right)$ becomes $\mathbf{1}$, a column vector with all elements set to unity, which means that the steering vector is equal to the ideal vector, i.e., $\mathbf{s}\left(\theta\right) = \mathbf{v}\left(\theta\right)$.

Owing to the single-valued relationship between azimuth and Doppler shown in (1), the independent variable in $\mathbf{s}\left(\theta\right)$, i.e., θ, can be replaced by f_d. Thus, after pulse compression in range domain and fast Fourier transformation (FFT) in azimuth domain with sufficient pulses (typically 256, 512, or more), the spatial snapshot in the Doppler bin with central frequency equal to f_d can be approximately given by a simplified expression as

$$\mathbf{x}\left(f_d\right) = a\left(f_d\right)\mathbf{s}\left(f_d\right) + \mathbf{n} \tag{4}$$

where the complex-valued scalar $a\left(f_d\right)$ denotes the Doppler spectral component corresponding to this Doppler bin and the complex-valued vector $\mathbf{n}$ represents the Gaussian noise component, which is independent cross-channel and with other components.

However, the signal model in (4) is only valid when the sampling rate in slow-time domain, i.e., the PRF, is large enough to fulfill the Nyquist sampling condition. With an insufficient PRF, spectrum aliasing will happen in Doppler domain, which means each Doppler bin may contain spectral components corresponding to more than one azimuth direction. In this case, the spatial snapshot in the Doppler bin with central frequency equal to f_d can be expressed as

$$\mathbf{x}\left(f_d\right) = \sum_{k=0}^{K-1} a\left(f_d + k \cdot f_{PRF}\right)\mathbf{s}\left(f_d + k \cdot f_{PRF}\right) + \mathbf{n} \tag{5}$$

where f_{PRF} represents the PRF and K denotes the total number of ambiguities. According to this model, the aim of ambiguity-free Doppler spectrum reconstruction in multi-channel HRWS-SAR can be described as to restore all the aliased spectral components, i.e., $a\left(f_d + k \cdot f_{PRF}\right)$, $k = 0, 1, \ldots, K-1$, from the original received data that is ambiguous in Doppler.

III. DOPPLER SPECTRUM RECONSTRUCTION APPROACHES AND THE INFLUENCE OF CHANNEL MISMATCH

As has been proved in many literatures [1]–[4], DBF technique gains the capability to accurately reconstruct the ambiguity-free Doppler spectrum for HRWS-SAR imaging. Among all the existing DBF methods, the kind with adaptive processing, referred to as ADBF or imaging STAP (ISTAP) [5]–[8], is currently recognized to be more applicable in practical processing. In these methods, cross-channel signal (the spatial snapshot) in each cell of the ambiguous range-Doppler (RD) spectrum is adaptively weighted, according to the statistical characteristics of the received data and based on certain optimum criterion, K times to extract all the K spectral components aliased in this cell. Regardless of different optimum criteria employed, nearly all the ADBF methods aim to maximally suppress the spectral components corresponding to undesired Doppler frequencies and keep the component corresponding to the desired Doppler frequency undistorted meanwhile.

Let $\mathbf{w}(f_d), \mathbf{w}(f_d + f_{PRF}), \cdots, \mathbf{w}(f_d + (K-1)\cdot f_{PRF})$ denote the adaptive weights employed to restore the spectral components corresponding to Doppler frequencies $f_d, f_d + f_{PRF}, \cdots, f_d + (K-1)\cdot f_{PRF}$, respectively. The reconstruction of ambiguity-free Doppler spectrum is then expressed as

$$\begin{aligned}
\tilde{a}(f_d) &= \mathbf{w}^H(f_d)\,\mathbf{x}(f_d) \\
\tilde{a}(f_d + f_{PRF}) &= \mathbf{w}^H(f_d + f_{PRF})\,\mathbf{x}(f_d) \\
&\vdots \\
\tilde{a}(f_d + (K-1)\cdot f_{PRF}) &= \mathbf{w}^H(f_d + (K-1)\cdot f_{PRF})\,\mathbf{x}(f_d)
\end{aligned} \tag{6}$$

where $\tilde{a}(f_d + k\cdot f_{PRF})$ denotes the reconstructed spectral component corresponding to Doppler frequency $f_d + k\cdot f_{PRF}$ and the superscript H is the operation of Hermitian transpose. In this paper, without loss of generality, the weights are calculated via the classical maximum signal-to-ambiguity-plus-noise ratio (SANR) criterion [8], which is obtained from

$$\begin{aligned}
&\mathbf{w}(f_d + k\cdot f_{PRF}) \\
&\quad = \frac{\mathbf{R}^{-1}(f_d)\,\mathbf{s}(f_d + k\cdot f_{PRF})}{\sqrt{\mathbf{s}^H(f_d + k\cdot f_{PRF})\,\mathbf{R}^{-1}(f_d)\,\mathbf{s}(f_d + k\cdot f_{PRF})}}, \\
&\quad k = 0, 1, \cdots, K-1
\end{aligned} \tag{7}$$

where $\mathbf{R}(f_d)$ is the covariance matrix of the Doppler bin with central frequency equal to f_d in the aliased data given by

$$\mathbf{R}(f_d) = E\left[\mathbf{x}(f_d)\,\mathbf{x}^H(f_d)\right] \tag{8}$$

with $E[\cdot]$ denoting the expectation operator. In practice, since $\mathbf{R}(f_d)$ is never known a priori, it is usually estimated by range averaging. As can be seen, the structure of the optimum weight vector in (7) is very similar to that of the weight vector used in jamming mitigation adaptive beamforming (ABF) or the weight used in STAP. While, for STAP, the interference is the clutter and jamming components, but the interference in SANR algorithm are the undesired spectral components corresponding to the aliased Doppler frequencies. The adaptive procedure in ADBF method allows for a more flexible spectrum reconstruction that can be implemented under a variety of system conditions, making this technique to be a more promising choice for HRWS-SAR imaging.

However, a key factor that degrades the performance of the ADBF algorithm is the mismatch between receiving channels, which is denoted by $\mathbf{g}(\theta)$ in (2). As pointed out by Ward [18], the structure of the optimum weight vector in (7) can be divided, according to different functions, into two cascaded parts. The first one is referred to as whiten filter (the inverse of covariance matrix), which whitens the receiving interference and thereby suppresses it to white noise level. The second is termed matched filter (the steering vector corresponding to the desired Doppler frequency), which protects the desired signal from distortion when it passes the spatial filter by constraining the main-lobe of the adaptive pattern to exactly point to the direction of the desired signal. Thus, any inaccuracy of the steering vector used in the weight vector will lead to a certain degree of distortion of the desired spectral component to be reconstructed. In fact, as is indicated in [30], even slight errors in the steering vector corresponding to the desired signal may result in severe degradation on the performance of ADBF when the desired signal is always present in the sample data (which is the case for the spectrum reconstruction in HRWS-SAR). Moreover, the distortions for all spectral components will be accumulated in the inverse fast Fourier transformation (IFFT) or other similar steps in SAR imaging procedure, leading to seriously deleterious effects on the quantity of data to be imaged. Therefore, to accurately reconstruct the ambiguity-free Doppler spectrum and acquire HRWS-SAR image with high quality, channel error should be well corrected a priori.

IV. NEW CHANNEL CALIBRATION ALGORITHM

In research field of multi-channel SAR and some other multi-channel receiving radar systems, channel calibration is an important issue that has long been investigated. A variety of mature methods have been proposed and tested via many experimental systems, such as the 2D frequency domain calibration method [15], the signal subspace projection algorithm [14], the principal eigenvector calibration approach [16], [17], and so on. For all these methods, a crucial underlying presumption is the Doppler-azimuth coupling effect shown in (1). Owing to this single-valued relationship between azimuth and Doppler, the azimuth-variant channel error can be estimated in Doppler domain (or image domain), and then can be calibrated. Nevertheless, all these methods tend to be invalid when they are used in multi-channel HRWS-SAR systems, since the single-valued Doppler-azimuth coupling effect is no longer valid due to the Doppler ambiguity.

In other words, the major reason for the inability of the above-mentioned calibration methods to process Doppler ambiguous data is the lack of ambiguity-free samples to be

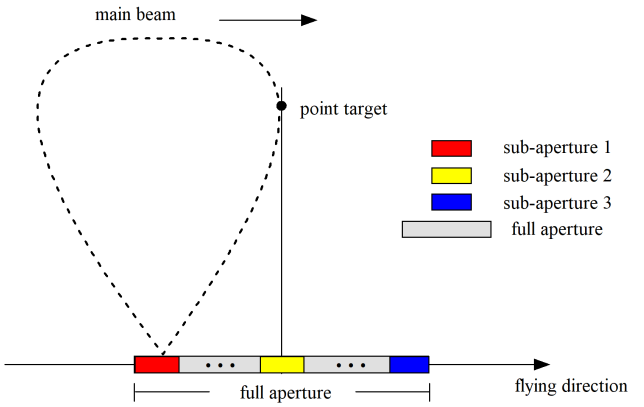

FIGURE 2. Two-dimensional echo collection geometry for the point target simulation.

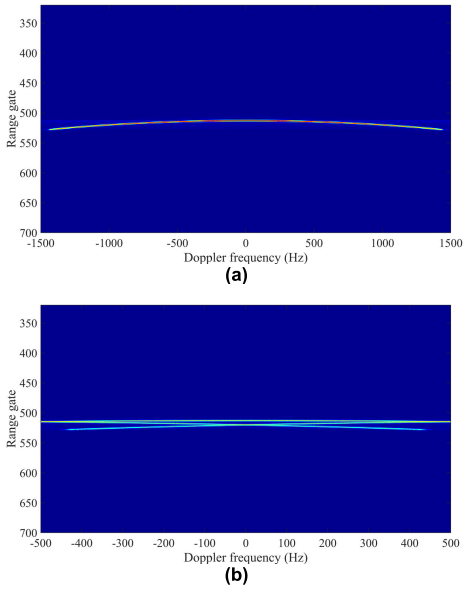

FIGURE 3. RD spectrums corresponding to the point target in full aperture. (a) The PRF is set to be 3000Hz. (b) The PRF is set to be 1000Hz.

used for channel error estimation. If one can find or extract a certain part of multi-channel data that is not aliased in Doppler, i.e., ambiguity-free sample data, it can be expected that these methods will regain their effectiveness when ultilized in HRWS-SAR system. Fortunately, we find that it is actually feasible. At least, by introducing sub-aperture operation, the multi-channel echo signal corresponding to isolated scatterers (point-like targets) in the scene to be imaged can be extracted without of Doppler ambiguity.

Here, we use point target (similar to isolated scatterer) simulation results to demonstrate how to extract the ambiguity-free multi-channel signal of isolated scatterer from the ambiguous data. The 2D echo collection geometry for this simulation is shown in Fig. 2. Note that, since our aim is to extract the multi-channel data of isolated scatterers (i.e., the echo signal of isolated scatterers collected by all the receiving channels simultaneously), any array processing operation cannot be used in this procedure. The full aperture for this point target (defined as the interval between the moment the target moves in the main beam and the moment it moves out) contains 16384 pulses, and the motion-induced Doppler bandwidth of this point target is about 2800Hz. Fig. 3 shows respectively the RD spectrums of the point target in the full aperture when sufficient and insufficient PRFs are considered. In Fig. 3 (a), since the PRF is set to be 3000Hz, which is greater than the Doppler bandwidth of the target, the RD spectrum is not aliased as expected. The PRF is then reduced to 1000Hz, which is equal to one third of that used in Fig. 3 (a), to generate the spectrum shown in Fig. 3 (b). It is clearly seen that the spectrum is aliased three times, with each Doppler bin containing spectral components corresponding to more than one actual Doppler center frequency, which implies that it is not an easy task to reconstruct the unambiguous spectrum of the target directly from the full aperture data.

To address this problem, sub-aperture processing is introduced herein, which divides the full aperture into small segments, with the length of each short enough (1024 pulse in this simulation). Thus, the Doppler bandwidth of the target in each sub-aperture is reduced to a low value much less than the PRF. Consequently, although the RD spectrum in each sub-aperture is still aliased in Doppler (since the sub-aperture division will not alter the sampling rate), the spectral components of the point target are no longer superimposed by themselves. In Fig. 4, the RD spectrums obtained from the three sub-apertures shown in Fig. 2 (sub-aperture 1∼3) are provided. As we can see, owing to the relatively small Doppler bandwidth, the majority of the spectral components corresponding to the target is not aliased in the spectrum. This is a very important precondition for us to reconstruct the unambiguous spectrum of this target.

Once we obtain all the sub-aperture RD spectrums, the next step is to increase the sampling rate and thus to reconstruct the ambiguity-free RD spectrum in each sub-aperture. We tackle this problem by zero-padding operations. Fig. 5 uses simplified RD spectrums corresponding to the three sub-apertures shown in Fig. 4 to demonstrate this procedure. By taking subfigure (a) as an example, we will illustrate the zero-padding operation in detail.

Since sub-aperture 1 is at the beginning of the full aperture (see Fig. 2), in which the flight is moving toward to the point target, the motion-induced Doppler frequencies in this aperture are positive-valued, as can be seen from the unambiguous RD spectrum in the first line. When the PRF is reduced three times, this spectrum is aliased (see the spectrum in the second line), with the part concerning the point target wrapping over to the position indicated by the dash arrow. By comparing the locations of the point target in the ambiguous and unambiguous spectrums, the positions where zeros should be put in the zero-padding operation can be clearly determined. As is depicted in the third line of this subfigure, zero-padding operation is applied to the left of the ambiguous spectrum, which extends the spectrum three times

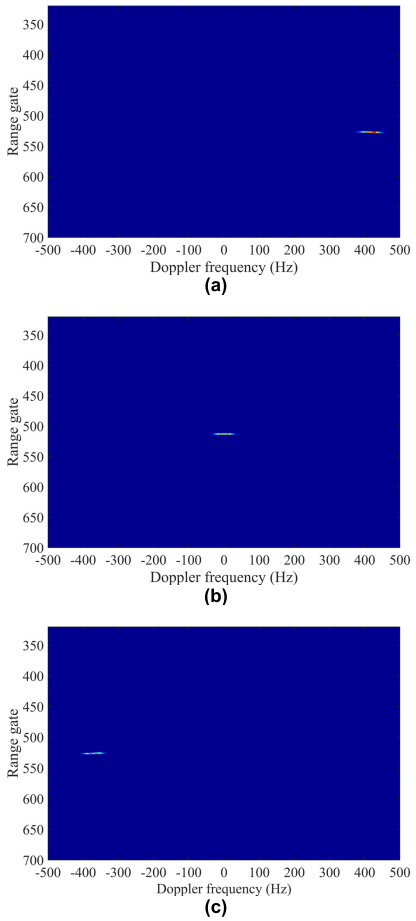

FIGURE 4. RD spectrums corresponding to the point target in sub-apertures. (a) Spectrum in sub-aperture 1. (b) Spectrum in sub-aperture 2. (c) Spectrum in sub-aperture 3.

(the sampling rate is increased three times). After comparing the extended spectrum with the unambiguous spectrum in the first line, it is obvious that the ambiguity-free RD spectrum of the point target is reconstructed. The similar procedures of zero-padding can also be seen from the other subfigures in Fig. 5.

After the zero-padding operations, all the extended sub-aperture data are transformed into slow-time domain via IFFT and are connected to each other according to the original order to regenerate the full aperture data. Then, slow-time domain FFT is again applied to the connected data to obtain the ambiguity-free RD spectrum in the full aperture. The signal processing flowchart of the complete reconstruction procedure is given in Fig. 6.

The above operations will be repeated in all the receiving channels to extract the ambiguity-free multi-channel spectrums of the point target. Since the Doppler ambiguity is eliminated, single-valued azimuth-Doppler coupling relationship is valid again, making the reconstructed multi-channel data well suitable to be used as samples to estimate channel error

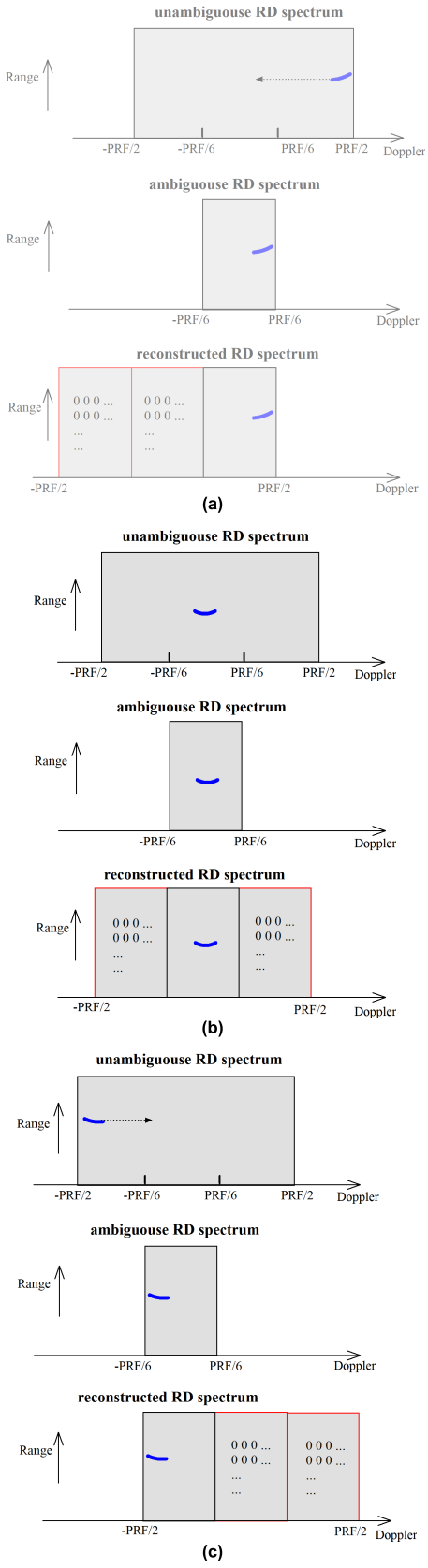

FIGURE 5. Demonstrations of RD spectrum reconstruction for point target. (a) Sub-aperture 1, (b) sub-aperture 2, (c) sub-aperture 3.

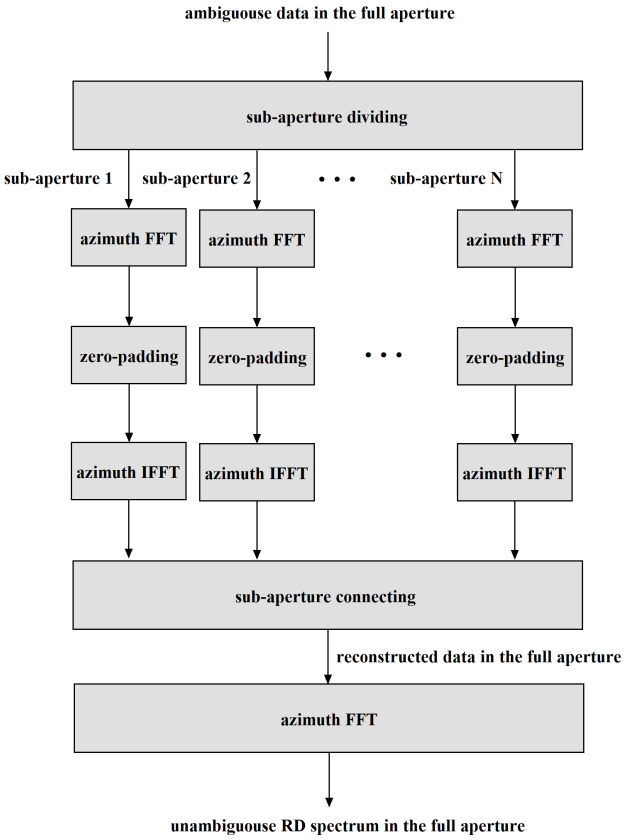

FIGURE 6. Flowchart of the spectrum reconstruction procedure for point-like target.

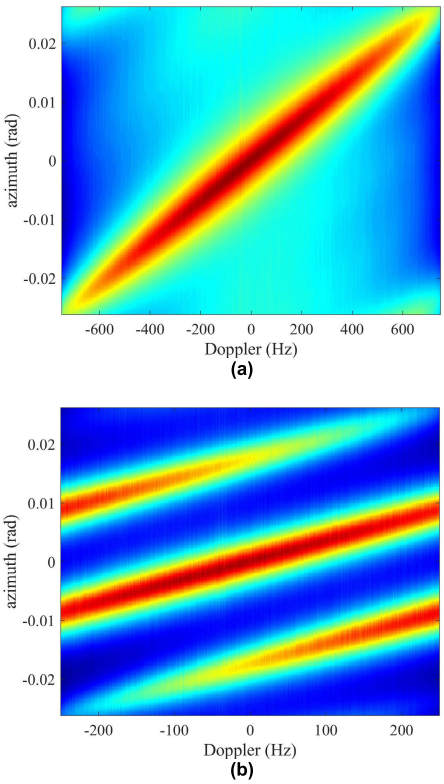

FIGURE 7. Two-dimensional MVDR spectrums of the measured data from the four-channel SAR system. (a) The spectrum is obtained before decimation (from the original data). (b) The spectrum is obtained after decimation.

TABLE 1. Parameters of the four-channel airborne SAR system.

Parameter	Value
Band	Ku
Number of receiving channels	4
Distance between receiving channels	0.25m
Bandwidth	1 GHz
Beam Width in Azimuth	3°
PRF (original)	1500Hz
PRF (after decimation)	500Hz
Number of coherent processing pulses (original)	24576
Number of coherent processing pulses (after decimation)	8192
Platform speed	80m/s
Platform altitude	6km
Distance between antenna phase center and scene center	15km

using traditional calibration method, such as the 2D frequency domain calibration algorithm [15], and the principal eigenvector calibration approach [16], [17].

Based on the analysis above, we propose here a new channel calibration algorithm for multi-channel HRWS-SAR, with the core steps described as below:

1. Divide the range compressed multi-channel data into several sub-apertures and apply azimuth FFT in each aperture independently to obtain sub-aperture RD spectrums. The length of each sub-aperture should be short enough to guarantee that the Doppler bandwidth of point-like target is relatively small as compared to the PRF. Usually, the length is chosen to ensure that the bandwidth of point-like target in each sub-aperture is less than one quarter or one eight of the PRF.

2. Find isolated scatterers (point-like targets) in sub-aperture RD spectrums, track them between adjacent apertures, and extract them from the apertures where they are tracked. In this paper, the traditional target detection algorithm, i.e., cell-averaging constant false alarm rate (CA-CFAR) detector, is employed to detect isolated scatterers over RD spectrums. Once a target is detected by the detector in several adjacent apertures, it will be recognized as an isolated scatterer to be processed in the following steps.

3. Reconstruct the ambiguity-free RD spectrums of all the isolated scatterers in full aperture by using the aforementioned method. Note that, as mentioned above, a key problem in this step is to determine the positions where zero-padding should be applied in each sub-aperture. In practice, the power and Doppler center of the isolated target between sub-apertures combined with the system parameters are employed to determine the positions where zeros should be put. The detailed description of this process will be given in the next section, where an example from measured data are used to demonstrate it more clearly.

4. Employ all the reconstructed spectrums of isolated targets in full aperture as samples to estimate and

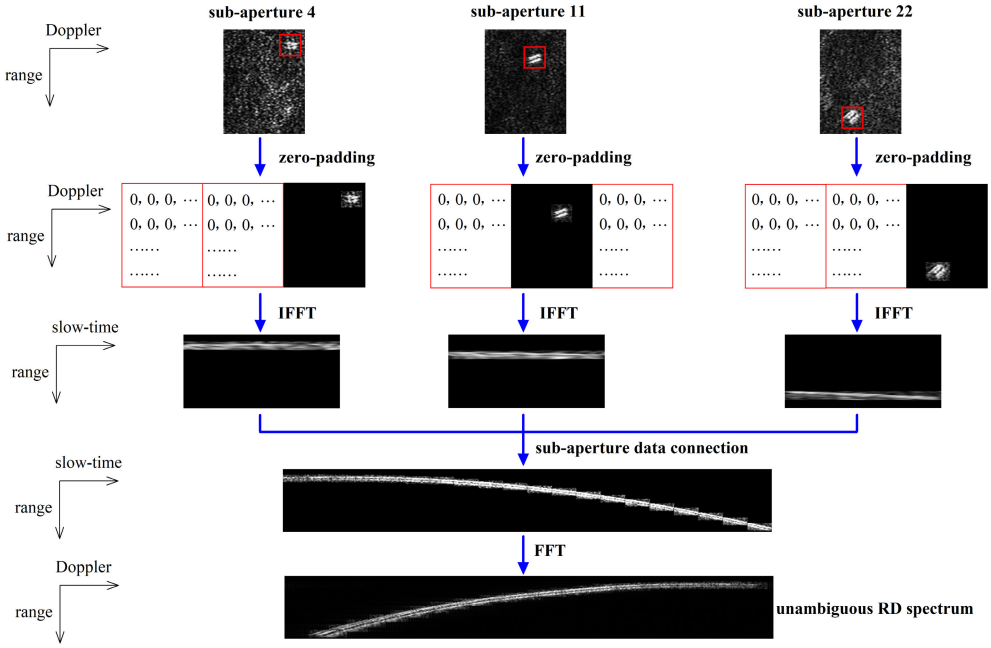

FIGURE 8. Demonstrations of ambiguity-free spectrum reconstruction for the isolated scatterer in real data.

calibrate channel error using traditional channel calibration method. In this paper, the principal eigenvector calibration approach [16], [17] is adopted, in which the estimation of the real steering vector is equal to the principal eigenvector, i.e., the eigenvector that corresponds to the maximal eigenvalue, of the sample covariance matrix generated by the reconstructed spectrums of isolated targets. Let $\hat{\mathbf{x}}_l\left(f_d + k \cdot f_{PRF}\right)$ denotes the reconstructed spectrum of the lth isolated target and L represents the total number of targets. The estimation of the real steering vector corresponding to Doppler frequency $f_d + k \cdot f_{PRF}$, denoted by $\tilde{\mathbf{s}}_l\left(f_d + k \cdot f_{PRF}\right)$, is obtained from

$$\tilde{\mathbf{s}}_l\left(f_d + k \cdot f_{PRF}\right) = \mathcal{P}\left\{\tilde{\mathbf{R}}\left(f_d + k \cdot f_{PRF}\right)\right\} \tag{9}$$

where $\mathcal{P}\{\cdot\}$ is the operator that yields the principal eigenvector of a matrix and $\tilde{\mathbf{R}}\left(f_d + k \cdot f_{PRF}\right)$ is the sample matrix corresponding to Doppler frequency $f_d + k \cdot f_{PRF}$, which is calculated from

$$\tilde{\mathbf{R}}\left(f_d + k \cdot f_{PRF}\right) = \frac{1}{L}\sum_{l=1}^{L}\hat{\mathbf{x}}_l\left(f_d + k \cdot f_{PRF}\right) \times \hat{\mathbf{x}}_l^H\left(f_d + k \cdot f_{PRF}\right). \tag{10}$$

As it will be verified by measured data in the next section, the proposed algorithm performs well and is robust to many kinds of channel errors in practical processing.

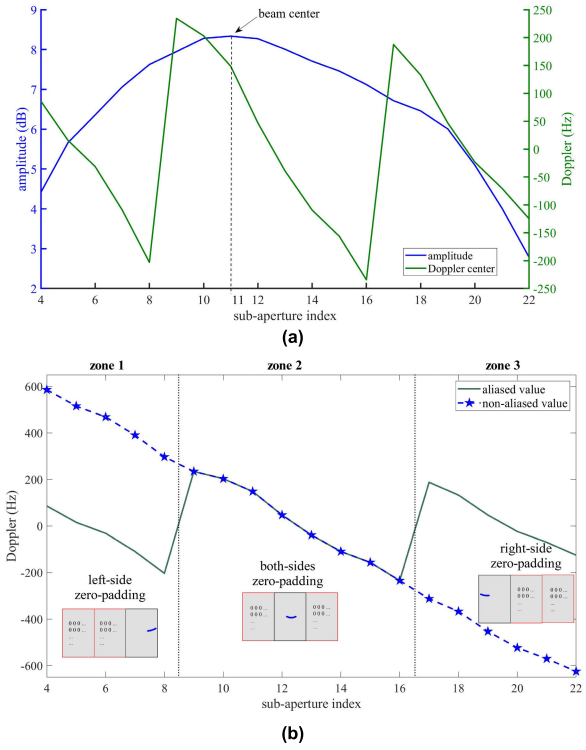

FIGURE 9. Demonstration of zero-padding. (a) Amplitude and Doppler center of the isolated scatterer versus sub-aperture index. (b) Aliased and real Doppler centers of the isolated scatterer versus sub-aperture index.

V. EXPERIMENTAL RESULTS

In this section, experimental results from two groups of measured data collected by multi-channel airborne SAR systems are provided to demonstrate how to extract ambiguity-free multi-channel signal of isolated scatterers and to validate the performance of the proposed calibration algorithm. It is obvious that the most suitable way to examine the performance of the proposed calibration algorithm is to compare the estimation of channel error to the real value. However, the

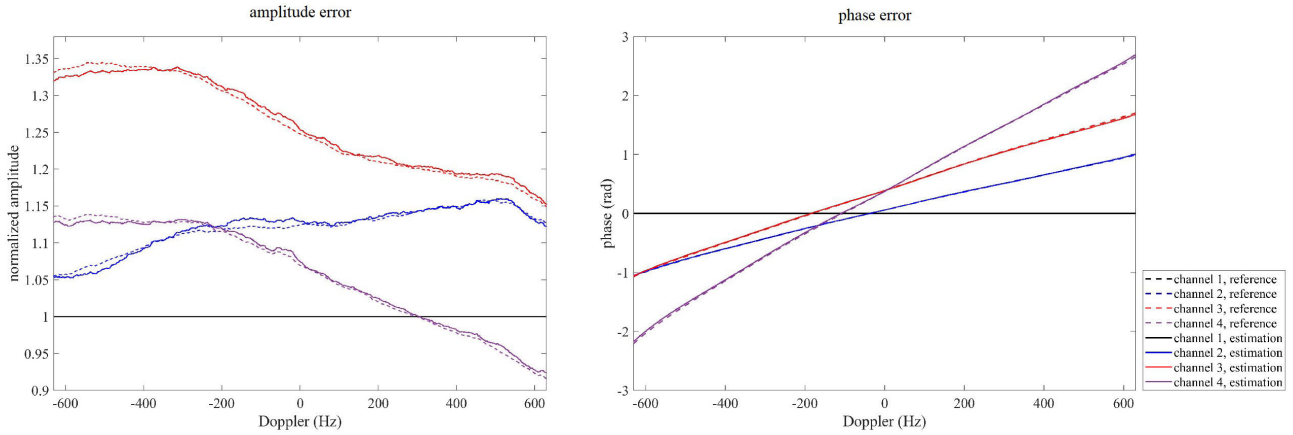

FIGURE 10. Estimated channel errors of the four-channel SAR system using ten samples.

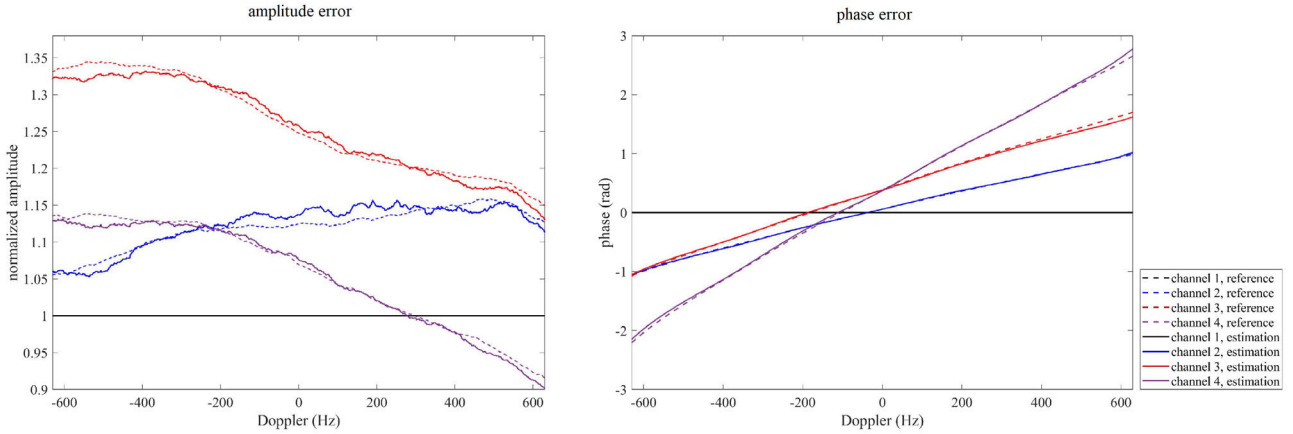

FIGURE 11. Estimated channel errors of the four-channel SAR system using four samples.

latter is hard to acquire in practice, since channel mismatch varies between different circumstances. Thus, instead of directly applying the proposed algorithm to Doppler ambiguous data, we first employ here a group of measured data that is Doppler ambiguity-free. The data is from a Ku-band airborne SAR system with four receiving channels. We first estimate the channel error from this data by the principal eigenvector calibration method [16], [17]. Since the data is unambiguous in Doppler, estimation with high accuracy can be achieved, which is recorded and then used, in lieu of the real but unknown channel error, as the reference in the following performance evaluation step.

After that, the unambiguous multi-channel data undergoes a three-time decimation processing (the PRF is reduced three times) to artificially generate Doppler ambiguous data, which is then used to test the proposed algorithm. The major parameters of the four-channel airborne SAR system are listed in Table 1, and the 2D minimum variance distortionless response (MVDR) spectrum concerning the measured data before and after decimation are shown in Fig. 7. By comparing the subfigures, it is clear that the decimated data is aliased in Doppler, with the total number of ambiguities equal to 3.

The ambiguous data is divided into 64 sub-apertures, each of which contains 128 pulses and undergoes azimuth FFT independently. Signal extraction of isolated scatterers is then applied over all the sub-apertures. To demonstrate how the ambiguity-free multi-channel signal of isolated scatterers can be reconstructed, an isolated scatterer that appears between the 4th sub-aperture and the 22th sub-aperture is taken as an example.

The entire procedure of ambiguity-free RD spectrum reconstruction for this isolated scatterer is depicted in Fig. 8. As we can see, the positions where the scatterer appears in different sub-apertures are labeled by red squares. By multiplying each of the sub-aperture spectrums to a 2D matrix (the same size of the sub-aperture spectrum) with the elements equal to 1 inside the red square and the elements equal to 0 outside the square, the majority of the signal corresponding to the isolated scatterer is extracted from the background.

The next step is the zero-padding operation on each sub-aperture RD spectrum, which aims to increase the sampling rate three times. A key issue in this step is to determine the positions where zeros should be padded, i.e., to which direction should the spectrums be extended. We use the

estimated amplitude and Doppler center of the extracted scatterer between sub-apertures combined with some of the system parameters to determine the zero-padding positions. In Fig. 9 (a), the blue and green curves show respectively the estimated amplitude and Doppler center of the scatterer versus sub-aperture index. As can be seen, due to the insufficient PRF, the curve of Doppler center is aliased three times. According to that, the sub-apertures are divided into three parts (three zones shown in Fig. 9 (b)). Let $\tilde{f}_{dc}(n)$ and $\hat{f}_{dc}(n)$ denote the aliased value (the value shown in the figure) and non-aliased value of the estimated Doppler center in the nth sub-aperture. We obtain

$$\hat{f}_{dc}(n) = \tilde{f}_{dc}(n) + k \cdot f_{PRF} \tag{11}$$

where k is an integer to be determine. It is obviously that the positions where zeros should be padded depend on the value of k. As we known, for a point-like target, the instantaneous Doppler frequency is a monotonic function of slow-time, which means the Doppler center of the scatterer is monotonic between sub-apertures. Consequently, once the value of k in any one of the sub-apertures is determined, the values of others can be deduced. In this paper, the value of k in the sub-aperture with the maximum amplitude of the scatterer is determined at first.

As is apparent in Fig. 9 (a), the amplitude of the isolated scatterer reaches its maximum value in the 11th sub-aperture, which implies that this sub-aperture is corresponding to the interval when the scatterer stays at the boresight of radar beam. Since the squint angle, i.e., the angle between the flight direction and the radar boresight, and the velocity of the flight is known a priori (at least, the approximate values of them are available), the real Doppler center of the scatterer in this sub-aperture, denoted by f_{dc}, can be calculated by

$$f_{dc} = \frac{2v_a \sin\theta_s}{\lambda} \tag{12}$$

Thus, the value of k in the sub-aperture with the maximum amplitude of the scatterer then can be obtained from

$$\min_k \left\{ \left| \tilde{f}_{dc}(n_{MA}) + k \cdot f_{PRF} - f_{dc} \right| \right\} \tag{13}$$

where n_{MA} is the index of the sub-aperture with the maximum amplitude of the scatterer ($n_{MA} = 11$ in this example).

Substituting the values of system parameters v_a, λ, and θ_s into (12), and the result back into (13), we obtain that the value of k in the 11th sub-aperture is equal to 0. Thus, it can be deduced that, in Fig. 9 (b), the values of k in sub-apertures of zone 1, 2, and 3 are equal to 1, 0, and -1, respectively. Based on that, the non-aliased curve of Doppler center is reconstructed, which is shown in Fig. 9 (b). By comparing the two curves, positions where zeros should be padded for each sub-aperture are determined (which is also depicted in this figure).

After that, all the extended sub-aperture RD spectrums are transformed into slow-time domain via azimuth IFFT, respectively, and then connected to generate the unambiguous data in the full aperture. Finally, azimuth FFT is applied in the full aperture to generate the Doppler ambiguity-free RD spectrum of this isolated scatterer, which is utilized as a sample to estimate the channel error using the principal eigenvector calibration method [16], [17].

(a)

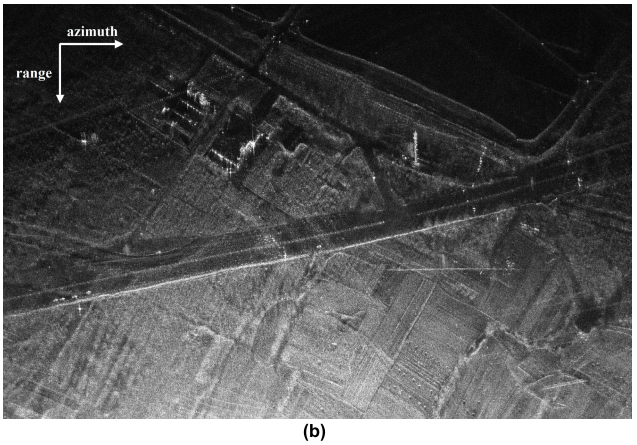

(b)

FIGURE 12. SAR images of the measured data from the four-channel SAR system. (a) Image generated from the original data. (b) Image generated from the reconstructed data.

TABLE 2. Parameters of the three-channel airborne SAR system.

Parameter	Value
Band	X
Number of receiving channels	3
Distance between receiving channels	0.35m
Bandwidth	100MHz
Beam Width in Azimuth	4.2°
total number of ambiguities	2
PRF	1000Hz
Number of coherent processing pulses	16384
Platform speed	150m/s
Platform altitude	5km
Distance between antenna phase center and scene center	24km

The estimation results of channel errors using the proposed algorithm are shown in Fig. 10, where the solid lines denote the estimated values and dash lines represent the reference values acquired from the original data. All the amplitude and phase errors corresponding to channel 2-4 are normalized with that of channel 1. That is the reason why the amplitude

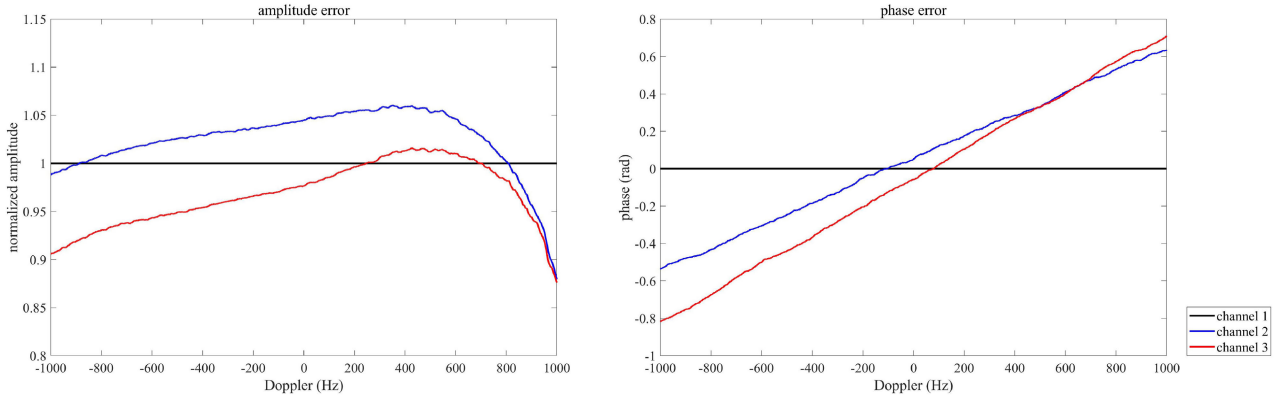

FIGURE 13. Estimated channel errors of the three-channel SAR system.

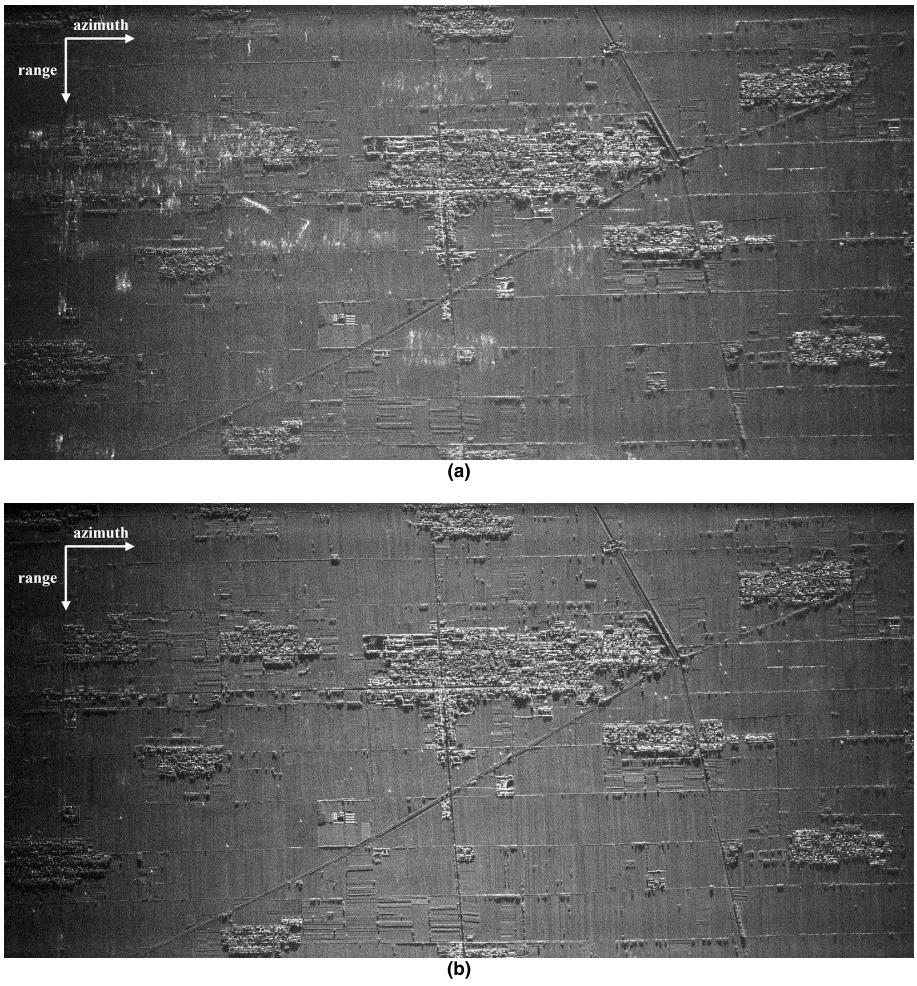

FIGURE 14. SAR images of the measured data from the three-channel SAR system. (a) Image generated without calibration. (b) Image generated with calibration.

and phase errors of channel 1 are constant values, equal to 1 for the amplitude and equal to 0 for the phase. All the curves are estimated via the principal eigenvector method with ten samples, i.e., extracted signal from ten isolated scatterers, and a low-pass filtering processing (smooth processing) is applied to all the curves to display them more clearly. As apparent from these figures, the gaps between the estimated values and the reference values of the amplitude and phase errors are negligible, especially for the phase errors shown in subfigure (b), where nearly perfect agreement of the estimated and reference values can be clearly recognized. These results indicate that an accurate estimation

of channel error can be achieved by using the proposed algorithm.

Considering that, under some circumstances, the imaging scenario appears to be homogeneous, with less isolated scatterers in it, the proposed algorithm is evaluated in case of less sample support. We reduce the number of samples (the extracted isolated scatterers) from ten to four and provide the estimation results in Fig. 11. No significant enlargement of the gaps between the estimated and reference curves can be recognized from these figures as compared to Fig. 10, which means that the accuracy of estimation maintains an acceptable level when the number of samples decreases from ten to four. The main reason is that the samples are all derived from isolated scatterers with, in general, strong power and high signal-to-noise ratio (SNR), which is beneficial for the precision of estimation.

After channel calibration, the maximum SANR ADBF method [8] is adopted on the four-channel data to reconstruct the ambiguity-free Doppler spectrum, which is then used to generate the final SAR image shown in Fig. 12. The classical ω-k imaging algorithm [31] and the long aperture autofocusing method [32] are employed in the procedure of imaging. The image generated from the original data (the unambiguous data before decimation) is also provided in subfigure (a) for comparison. As we can see, except for a few undesired residues corresponding to extremely strong scatterers in subfigure (b), the difference between the images generated from the reconstructed data and the original data are not evident actually, which also validates the effectiveness of the proposed calibration algorithm.

To further test the performance in practice, the proposed calibration algorithm is then adopted to process a group of measured data that is ambiguous in Doppler. The data is collected by a three-channel airborne SAR system, whose major parameters are listed in Table 2. Since the main purpose of the data collection is to test the performance of HRWS imaging for multi-channel SAR, a relatively small PRF is selected, which causes a two-times ambiguity in Doppler.

Fig 13 shows the channel errors of this dataset estimated by using the proposed algorithm. Ten isolated scatterers (samples) are extracted for the estimation. In Fig. 14, the final HRWS SAR images with and without channel calibration are provided for comparison. By comparing the two images, it is clear that the proposed calibration algorithm has the ability to accurately calibrate channel mismatch of multi-channel HRWS-SAR system in case of Doppler ambiguity, resulting in a significant improvement in the quality of the final SAR images.

VI. CONCLUSION

Accurate calibration of imbalance between receiving channels for multi-channel HRWS-SAR system is never an easy task, as the traditional multi-channel SAR calibration methods depending on the single-valued azimuth-Doppler coupling relationship become invalid due to Doppler ambiguity. To remedy this, this paper proposed a new channel calibration algorithm for multi-channel HRWS-SAR. Instead of using signal subspace projection or other matrix analysis methods, it intends to find samples of multi-channel signal that is totally ambiguity-free to make the traditional multi-channel SAR channel calibration methods suitable for HRWS-SAR system. We demonstrate that, by sub-aperture processing, it is completely feasible to extract ambiguity-free multi-channel signal corresponding to isolated scatterers from the Doppler ambiguous data. These extracted signal are transformed into RD domain and then used as samples to estimate the channel error via traditional calibration method. As verified by two groups of measured data collected by two airborne multi-channel SAR systems, the proposed algorithm can accurately calibrate the azimuth-variant channel mismatch for multi-channel HRWS-SAR system when Doppler ambiguity occurs. Moreover, it is also proved that, the proposed algorithm can achieve acceptable calibration performance even with less sample support, making it robust to many imaging scenarios in practical applications.

REFERENCES

[1] G. Krieger, N. Gebert, and A. Moreira, "Unambiguous SAR signal reconstruction from nonuniform displaced phase center sampling," *IEEE Geosci. Remote Sens. Lett.*, vol. 1, no. 4, pp. 260–264, Oct. 2004.
[2] N. Gebert, G. Krieger, and A. Moreira, "Digital beamforming on receive: Techniques and optimization strategies for high-resolution wide-swath SAR imaging," *IEEE Trans. Aerosp. Electron. Syst.*, vol. 45, no. 2, pp. 564–592, Apr. 2009.
[3] N. Gebert, G. Krieger, and A. Moreira, "Multichannel azimuth processing in ScanSAR and TOPS mode operation," *IEEE Trans. Geosci. Remote Sens.*, vol. 48, no. 7, pp. 2994–3008, Jul. 2010.
[4] J.-H. Kim, M. Younis, A. Moreira, and W. Wiesbeck, "Spaceborne MIMO synthetic aperture radar for multimodal operation," *IEEE Trans. Geosci. Remote Sens.*, vol. 53, no. 5, pp. 2453–2466, May 2015.
[5] Z. Li, H. Wang, T. Su, and Z. Bao, "Generation of wide-swath and high-resolution SAR images from multichannel small spaceborne SAR systems," *IEEE Geosci. Remote Sens. Lett.*, vol. 2, no. 1, pp. 82–86, Jan. 2005.
[6] L. Zhenfang, B. Zheng, W. Hongyang, and L. Guisheng, "Performance improvement for constellation SAR using signal processing techniques," *IEEE Trans. Aerosp. Electron. Syst.*, vol. 42, no. 2, pp. 436–452, Apr. 2006.
[7] D. Cerutti-Maori, I. Sikaneta, and C. H. Gierull, "Optimum SAR/GMTI processing and its application to the radar satellite RADARSAT-2 for traffic monitoring," *IEEE Trans. Geosci. Remote Sens.*, vol. 50, no. 10, pp. 3868–3881, Oct. 2012.
[8] D. Cerutti-Maori, I. Sikaneta, J. Klare, and C. H. Gierull, "MIMO SAR processing for multichannel high-resolution wide-swath radars," *IEEE Trans. Geosci. Remote Sens.*, vol. 52, no. 8, pp. 5034–5055, Aug. 2014.
[9] J.-H. Kim, A. Ossowska, and W. Wiesbeck, "Experimental investigation of digital beamforming SAR performance using a ground-based demonstrator," in *Proc. IEEE Int. Geosci. Remote Sens. Symp.*, Barcelona, Spain, Jul. 2007, pp. 111–114.
[10] N. Gebert, F. Q. De Almeida, and G. Krieger, "Airborne demonstration of multichannel SAR imaging," *IEEE Geosci. Remote Sens. Lett.*, vol. 8, no. 5, pp. 963–967, Sep. 2011.
[11] J.-H. Kim, M. Younis, P. Prats-Iraola, M. Gabele, and G. Krieger, "First spaceborne demonstration of digital beamforming for azimuth ambiguity suppression," *IEEE Trans. Geosci. Remote Sens.*, vol. 51, no. 1, pp. 579–590, Jan. 2013.
[12] D. Cerutti-Maori and I. Sikaneta, "A generalization of DPCA processing for multichannel SAR/GMTI radars," *IEEE Trans. Geosci. Remote Sens.*, vol. 51, no. 1, pp. 560–572, Jan. 2013.
[13] I. Sikaneta and D. Cerutti-Maori, "Demonstrations of HRWS and GMTI with RADARSAT-2," in *Proc. 9th Eur. Conf. Synth. Aperture Radar*, Nuremberg, Germany, Apr. 2012, pp. 263–266.
[14] M. Soumekh, "Moving target detection in foliage using along track monopulse synthetic aperture radar imaging," *IEEE Trans. Image Process.*, vol. 6, no. 8, pp. 1148–1163, Aug. 1997.

[15] J. Ender, "The Airborne Experimental Multi-Channel SAR-System AER-?" in *Proc. EUSAR Conf.*, Königswinter, Germany, May 1996, pp. 49–52.
[16] J. Ender, "Detection and estimation of moving target signals by multichannel SAR," *AEÜ Int. J. Electron. Commun.*, vol. 50, no. 2, pp. 150–156, 1996.
[17] W.-D. Wirth, *Radar Techniques Using Array Antennas*. London, U.K.: Institution of Electrical Engineers, 2001.
[18] J. Ward, "Space-time adaptive processing for airborne radar," MIT Lincoln Lab., Lexington, MA, USA, Tech. Rep. ESC1015, 1994.
[19] L. Zhang, M. D. Xing, C. W. Qiu, and Z. Bao, "Adaptive two-step calibration for high-resolution and wide-swath SAR imaging," *IET Radar, Sonar Navigat.*, vol. 4, no. 4, pp. 548–559, Aug. 2010.
[20] L. Aifei, L. Guisheng, M. Lun, and X. Qing, "An array error estimation method for constellation SAR systems," *IEEE Geosci. Remote Sens. Lett.*, vol. 7, no. 4, pp. 731–735, Oct. 2010.
[21] S.-X. Zhang, M.-D. Xing, X.-G. Xia, Y.-Y. Liu, R. Guo, and Z. Bao, "A robust channel-calibration algorithm for multi-channel in azimuth HRWS SAR imaging based on local maximum-likelihood weighted minimum entropy," *IEEE Trans. Image Process.*, vol. 22, no. 12, pp. 5294–5305, Dec. 2013.
[22] S.-X. Zhang, M.-D. Xing, X.-G. Xia, L. Zhang, R. Guo, Y. Liao, and Z. Bao, "Multichannel HRWS SAR imaging based on range-variant channel calibration and multi-Doppler-direction restriction ambiguity suppression," *IEEE Trans. Geosci. Remote Sens.*, vol. 52, no. 7, pp. 4306–4327, Jul. 2014.
[23] J. Feng, C. Gao, Y. Zhang, and R. Wang, "Phase mismatch calibration of the multichannel SAR based on azimuth cross correlation," *IEEE Geosci. Remote Sens. Lett.*, vol. 10, no. 4, pp. 903–907, Jul. 2013.
[24] Y. Liu, Z. Li, Z. Wang, and Z. Bao, "On the baseband Doppler centroid estimation for multichannel HRWS SAR imaging," *IEEE Geosci. Remote Sens. Lett.*, vol. 11, no. 12, pp. 2050–2054, Dec. 2014.
[25] C. Fang, Y. Liu, Z. Suo, Z. Li, and J. Chen, "Improved channel mismatch estimation for multi-channel HRWS SAR based on azimuth cross-correlation," *Electron. Lett.*, vol. 54, no. 4, pp. 235–237, Feb. 2018.
[26] T. Yang, Z. Li, Y. Liu, and Z. Bao, "Channel error estimation methods for multichannel SAR systems in azimuth," *IEEE Geosci. Remote Sens. Lett.*, vol. 10, no. 3, pp. 548–552, May 2013.
[27] Y.-Y. Liu, Z.-F. Li, T.-L. Yang, and Z. Bao, "An adaptively weighted least square estimation method of channel mismatches in phase for multichannel SAR systems in azimuth," *IEEE Geosci. Remote Sens. Lett.*, vol. 11, no. 2, pp. 439–443, Feb. 2014.
[28] Z. Wang, Y. Liu, Z. Li, G. Xu, and J. Chen, "Phase bias estimation for multi-channel HRWS SAR based on Doppler spectrum optimisation," *Electron. Lett.*, vol. 52, no. 21, pp. 1805–1807, Oct. 2016.
[29] P. Huang, X.-G. Xia, X. Liu, X. Jiang, J. Chen, and Y. Liu, "A novel baseline estimation method for multichannel HRSW SAR system," *IEEE Geosci. Remote Sens. Lett.*, to be published. doi: 10.1109/LGRS.2019.2911735.
[30] D. D. Feldman and L. J. Griffiths, "A projection approach for robust adaptive beamforming," *IEEE Trans. Signal Process.*, vol. 42, no. 4, pp. 867–876, Apr. 1994.
[31] I. Cumming and F. Wong, *Digital Processing of Synthetic Aperture Radar Data*. Norwood, MA, USA: Artech House, 2005.
[32] D. Zhu, R. Jiang, X. Mao, and Z. Zhu, "Multi-subaperture PGA for SAR autofocusing," *IEEE Trans. Aerosp. Electron. Syst.*, vol. 49, no. 1, pp. 468–488, Jan. 2013.

DI WU was born in Anyang, China, in 1982. He received the B.S. degree in information engineering and the Ph.D. degree in communication and information systems from the Nanjing University of Aeronautics and Astronautics (NUAA), Nanjing, China, in 2005 and 2011, respectively.

In 2011, he joined the College of Electronic and Information Engineering and the Key Laboratory of Radar Imaging and Microwave Photonics, Ministry of Education, NUAA, where he is currently an Associate Professor. From 2018 to 2019, he was a Visiting Scholar with the Department of Informatics, University of Leicester, U.K. His current research interests include radar imaging algorithms, space–time adaptive processing (STAP), and SAR ground moving target indication (SAR/GMTI).

YUDONG ZHANG received the B.Sc. degree (Hons.) and the three-year M.Phil. degree from the Nanjing University of Aeronautics and Astronautics (NUAA), China, and the Ph.D. degree in signal and information processing from Southeast University, China, in 2010. He held a postdoctoral position with Columbia University, from 2010 to 2012, and was an Assistant Research Scientist with the Research Foundation of Mental Hygiene (RFMH) affiliated with Columbia University, from 2012 to 2013. He served as a Professor with Nanjing Normal University (NJNU), from 2013 to 2017, where he was the Director and the Founder of the Advanced Medical Image Processing Group. Since 2018, he has been a Professor with the Department of Informatics, University of Leicester, U.K.

DAIYIN ZHU was born in Wuxi, China, in 1974. He received the B.S. degree in electronic engineering from Southeast University, Nanjing, China, in 1996, and the M.S. and Ph.D. degrees in electronics from the Nanjing University of Aeronautics and Astronautics (NUAA), Nanjing, in 1998 and 2002, respectively.

From 1998 to 1999, he was a Guest Scientist with the Institute of Radio Frequency Technology, German Aerospace Center, Oberphaffenhofen, where he was involved in SAR interferometry. In 1998, he joined the Department of Electronic Engineering, NUAA, where he is currently a Professor. He has developed algorithms for several operational airborne SAR systems. His current research interests include radar imaging algorithms, SAR/ISAR autofocus techniques, SAR ground moving target indication (SAR/GMTI), and SAR interferometry.

SHUIHUA WANG received the B.S. degree from Southeast University, in 2008, the M.S. degree from The City University of New York, in 2012, and the Ph.D. degree from Nanjing University, in 2017. She was a Research Assistant with Columbia University, from 2012 to 2014. She was a Research Associate with Loughborough University, from 2018 to 2019. She is currently a Research Fellow with the University of Leicester. She published over 100 articles in SCI-indexed journals. She has been serving as an Editor for IEEE Access and the *Journal of Alzheimer's Disease*, since 2018, and was the Managing Guest Editor for *Multimedia Tools and Applications*, from 2017 to 2018.

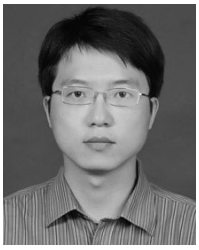

MINGWEI SHEN received the B.S. and Ph.D. degrees in electronic engineering from the Nanjing University of Aeronautics and Astronautics (NUAA), Nanjing, in 2003 and 2008, respectively. Since 2011, he has been with the College of Computer and Information Engineering, Hohai University, where he is currently an Associate Professor. He published more than 50 contributory articles in referred journals and international conference proceedings. His current research interests include space–time adaptive processing (STAP) and SAR ground moving target indication (SAR/GMTI).